Estimating the CO_2 fertilization effect on extratropical forest productivity from Flux-tower observations

Chunhui Zhan[1,2], René Orth[1,3], Hui Yang[1], Markus Reichstein[1], Sönke Zaehle[1], Martin G. De Kauwe[4], Anja Rammig[2] and Alexander J. Winkler[1]

[1] Max Planck Institute for Biogeochemistry, 07745 Jena, Germany

[2] School of Life Sciences, Technical University of Munich, 85354 Freising, Germany

[3] Faculty of Environment and Natural Resources, University of Freiburg, 79106 Freiburg, Germany

[4] School of Biological Sciences, University of Bristol, BS8 1TQ Bristol, UK

Corresponding author: Chunhui Zhan (czhan@bgc-jena.mpg.de)

Key Points:

- We present a novel statistical method to disentangle the variability of photosynthetic rates related to climate and non-climate drivers
- The analysis from 38 eddy covariance sites shows a 16.4 ± 4% increase in photosynthetic carbon uptake for a 100 ppm rise in atmospheric CO_2
- Our statistical method is successfully validated against idealized model simulations with and without increasing CO_2

Abstract

The land sink of anthropogenic carbon emissions, a crucial component of mitigating climate change, is primarily attributed to the CO_2 fertilization effect on global gross primary productivity (GPP). However, direct observational evidence of this effect remains scarce, hampered by challenges in disentangling the CO_2 fertilization effect from other long-term drivers, particularly climatic changes. Here, we introduce a novel statistical approach to separate the CO_2 fertilization effect on GPP and daily maximum net ecosystem production (NEP_{max}) using eddy covariance records across 38 extratropical forest sites. We find the median stimulation rate of GPP and NEP_{max} to be 16.4 ± 4% and 17.2 ± 4% per 100 ppm increase in atmospheric CO_2 across these sites, respectively. To validate the robustness of our findings, we test our statistical method using factorial simulations of an ensemble of process-based land surface models. We acknowledge that additional factors, including nitrogen deposition and land management, may impact plant productivity, potentially confounding the attribution to the CO_2 fertilization effect. Assuming these site-specific effects offset to some extent across sites as random factors, the estimated median value still reflects the strength of the CO_2 fertilization effect. However, disentanglement of these long-term effects, often inseparable by timescale, requires further causal research. Our study provides direct evidence that the photosynthetic stimulation is maintained under long-term CO_2 fertilization across multiple eddy covariance sites. Such observation-based quantification is key to constraining the long-standing uncertainties in the land carbon cycle under rising CO_2 concentrations.

Plain Language Summary

Through photosynthesis, plants convert CO_2 and water into sugars and oxygen using solar energy, one of the most important chemical reactions on Earth. Human-made carbon emissions are increasing increasing atmospheric CO_2 levels, impacting global photosynthesis. The additional carbon is believed to have a fertilizing effect on photosynthesis, causing vegetation to absorb a significant portion of the emitted CO_2. However, the strength of this CO_2 fertilization effect on photosynthesis is uncertain, but is a crucial factor in determining the future trajectory of atmospheric CO_2 concentrations. In this study, we introduce a new statistical method to quantify the increase in photosynthetic carbon uptake, stimulated by rising CO_2, based on measurements from 38 forest sites. Our results reveal that a 100 ppm increase in CO_2 enhances photosynthesis by approximately 16%. Validation of the statistical method with artificial model experiments

supports the robustness of our findings. Our study improves the understanding of the impacts of human-made CO_2 emissions on the global carbon cycle.

1 Introduction

Forests play a crucial role in the global carbon cycle, acting as a significant sink for anthropogenic carbon emissions. Approximately 25% of annual carbon emissions are estimated to be sequestered and stored by forests via photosynthesis, with boreal and temperate forests making substantial contributions (Pan et al., 2011). The physiological effects of increasing atmospheric carbon dioxide (CO_2) on plant productivity, known as the CO_2 fertilization effect, are expected to stimulate photosynthesis and drive the enhanced carbon uptake. However, obtaining observational evidence for these effects in natural ecosystems and understanding how this process has changed historically remains a key knowledge gap.

Multiple lines of evidence support an enhancement in photosynthesis (or gross primary production; GPP) in response to an increase in CO_2: CO_2 enrichment experiments (Norby et al., 2010; Walker et al., 2021), ecosystem monitoring (Keenan et al., 2013; Fernández-Martínez et al., 2017; Mastrotheodoros et al., 2017) and indirect proxies based on long-term atmospheric carbonyl sulfide records (Campbell et al., 2017) or isotopomer signal (Ehlers et al., 2015). Process-based land-surface models, which simulate the physiological responses of vegetation to environmental changes, also predict a stimulation of photosynthesis with increasing CO_2 levels (Sitch et al., 2015). However, multi-model projections of the CO_2 effect on long-term GPP diverge considerably due to uncertainties in process parameterizations and feedback mechanisms, particularly in response to meteorological extremes and climatic changes associated to rising CO_2 (Zaehle et al., 2005; De Kauwe et al., 2013; Rogers et al., 2014). Constraining the CO_2 fertilization effect in models through direct observational evidence is a long-called-for necessity to advance our understanding of carbon cycling and essential for more reliable future projections of carbon sequestration.

The global network of eddy covariance (EC) flux towers observing the exchange of CO_2 at the ecosystem scale provides a valuable resource, as it has accumulated sufficiently long time series data to potentially provide direct evidence of the CO_2 fertilization effect (Knauer et al., 2017; Baldocchi, 2020; Zhan et al., 2022). Previous studies have attempted to attribute the CO_2 fertilization effect on GPP by utilizing EC records. However, these studies have not adequately

accounted for confounded drivers of GPP, potentially leading to a misattribution, or only relied on an indirect use of measurements for attribution, such as using EC data to calibrate a predefined model. For instance, (Chen et al., 2022) used an eco-evolutionary optimality framework to reproduce EC-inferred GPP and subsequently attribute the CO_2 fertilization effect on GPP. Their analysis estimated a global GPP enhancement of 63 g C m^{-2} yr^{-1} from 2001-2014 due to rising CO_2. Similarly, (Ueyama et al., 2020) utilized a model constrained with data from 104 EC towers and estimated a 12.4 g C m^{-2} yr^{-1} increase in GPP. (Fernández-Martínez et al., 2017), employing generalized mixed linear models, attributed an increase of 11.2 ± 2.5 g C m^{-2} yr^{-1} in the GPP from 1995-2011 at 23 forest sites to CO_2. These variations emphasize the importance of disentangling the CO_2 effect on GPP directly, *i.e., not using predefined model structures*, and by carefully considering confounding drivers in leveraging the continuously growing EC records.

In this study, we aim to disentangle the CO_2 fertilization effect on photosynthetic uptake directly and exclusively from long-term multi-site flux measurements and accompanying meteorological data. Several factors, such as CO_2, climate changes, land-use and land-cover changes, affect ecosystem productivity and are correlated and confounded on the multi-decadal time-scale. We introduce the so-called *GPP residual method* that statistically captures the sensitivity of GPP to CO_2 and climate variables at different time scales to account for co-linearities among the drivers. First, we detrend the GPP time series to separate the long-term variability of GPP (the trend) primarily driven by CO_2 and climate, from the shorter-term variability (anomalies) primarily driven by climate variabilities. The method estimates the sensitivity of GPP to climate, referred to as the γ effect with temperature change as the proxy for climatic change, based on these anomalies. Next, we can quantify the γ effect based on long-term changes assuming the sensitivity remains consistent over the time scales of a few decades. The difference between the original observed GPP trend and the inferred GPP trend due to climate changes yields the unexplained GPP residual, which can be attributed to the long-term CO_2 effect on GPP, here referred to as the β effect. Specifically, we define the β factor as the relative change in GPP (%) per 100 ppm increase in CO_2, and the γ factor as the relative change in GPP (%) per Kelvin increase in surface air temperature. It's important to note that the GPP residual may also include other long-term effects specific to individual sites, such as signals related to nitrogen deposition or land management. First, we validate the robustness of the *GPP residual method* using site-

level simulations with the QUINCY model (QUantifying Interactions between terrestrial Nutrient CYcles and the climate system; Thum et al., 2019). We use the *GPP residual method* to further estimate the β and γ effects in both GPP and daily maximum net ecosystem production (NEP_{max}) using long-term EC records. At last, we compare the results from EC records and factorial simulations from a set of land-surface models (TRENDY version 9; Sitch et al., 2015). Additionally, we discuss the relevance of other potential long-term impacts on GPP in more detail.

2 Materials and Methods

2.1 Eddy covariance data

This study comprises 38 forested eddy covariance (EC) sites (Table S1), where CO_2 flux data and meteorological data are collected by flux towers from Integrated Carbon Observation System (ICOS; Rebmann et al., 2018), and AmeriFlux (Novick et al., 2018). We focus on tree-dominated ecosystems as they exhibit less sensitivity to short-term climate variability compared to grass-dominated ecosystems. We focus on tree-dominated ecosystems due to the heightened sensitivity of grass-dominated ecosystems to short-term climate variability, adding complexity to the disentanglement of their response to CO_2 (Hovenden et al., 2014; Reich et al., 2018). The sites span geographically across Europe and North America. The forest types can be broadly classified into: deciduous broadleaf forest (DBF; 12 sites), evergreen need-leaved forest (ENF; 20 sites), and mixed deciduous–coniferous forest (MF; 6 sites).

We obtain long-term recorded (≥10 years) eddy covariance data at daily scale and net ecosystem production (NEE) at half-hourly scale from 1994 to 2022 (Table S2). GPP is estimated from the nighttime partitioning algorithm (Reichstein et al., 2005) . Meteorological variables used in this study include temperature, incoming shortwave radiation and vapour pressure deficit (VPD). Due to the limited depth of soil moisture measurements (Yu et al., 2022), we calculate a water availability index (WAI; Tramontana et al., 2016) following a bucket model approach. The maximum cumulative water deficit (Aragão et al., 2007) represents the available water content (awc). WAI is calculated as the balance of precipitation recharge and observed evapotranspiration as follows:

$$input(t) = \min\left(Precipitation(t), awc - WAI(t)\right) \quad (1)$$

$$WAI\ (t+1) = \max\left(\left(WAI(t) + \ input(t) - Evapotranspiration(t)\right), 0\right) \quad (2)$$

Where t represents the timestep t. We exclusively include data with daily quality control indicators for NEE and meteorological variables surpassing 0.6, denoting a 60% or higher percentage of measured and high-quality gap-filled data. In summary, EC sites are selected for this study based on three criterias: (a) only sites dominated by tree-ecosystems are selected; (b) there has to be a long-term record of EC observations (≥10 years) after the quality control when (c) at least 60% data per day is measured or gap-filled with good quality. In total we estimate β and γ for 228 site-months.

Maximum leaf area index (LAI_{max}, $m^2\ m^{-2}$), forest age (years), site-specific disturbance or management information are collected from the literature (Musavi et al., 2017; Besnard et al., 2018; Flechard et al., 2020; Migliavacca et al., 2021), the BADM product, and/or site principal investigators.

Due to the systematic biases of the atmospheric CO_2 measurements in the eddy covariance data, for consistency, we replace the CO_2 measurement with the CO_2 product CAMS CF-1.6 (Chevallier et al., 2005, 2010) from the nearest pixel to each EC site. The CO_2 reanalysis data spans from 1994 to 2022 with daily resolution, thus sufficient to match the time period of the eddy covariance data.

2.2 Estimating β and γ using the *GPP residual method*

We develop the *GPP residual method* (Figure 1) to isolate the CO_2 fertilization effect (β) from other confounding factors (*e.g., climate*). β is inferred for each site and each month-of-year separately, using the median values of GPP and hydro-meteorological data across five-day intervals within the considered months to filter out synoptic weather variability and its impact on GPP dynamics. The calculation of β consists of three steps: (1) Data preparation (Figure 1b). The growing season when plant photosynthesis is active is defined based on the mean seasonal cycle of GPP (averages by day-of-year) across the time series. A month is considered within the growing season, if there are more than twenty days when GPP is greater than 25% of the

maximum of GPP as inferred from the mean seasonal cycle. Within each month, the median values of all variables are retrieved for every five-day interval. We then calculate anomalies using the median values by subtracting the long-term trend of the linear-fit for each month-of-year (*e.g., July in 1999, …,2020*). We rescale the anomalies of all variables by adding the average value across the considered time period. The rescaling allows the random forest model in step (2) is trained and applied at an identical magnitude to extrapolate; (2) Model training and predicting climatic effects on GPP (Figure 1c). We train a random forest regression model for GPP anomalies using anomalies of hydro-meteorological variables (*i.e., temperature (Temp), incoming shortwave radiation (SW_{in}), vapor pressure deficit (VPD), water availability index (WAI), growing degree days (GDD)*). We use the model to predict GPP using the actual hydro-meteorological data (including both trends and anomalies) at each month-of-year. The predicted GPP ($GPP_{climatic}$) thus only reflects the effect of climate. Next to the random forest regression model, we call a multivariate linear regression model to test the robustness of the results from the random forest regression model (Figure S1); (3) Isolating non-climatic effects on GPP (Figure 1d). The non-climatic effects on GPP ($GPP_{residual}$) are derived by removing the $GPP_{climatic}$ from the actual GPP time series ($GPP_{residual}$ = GPP - $GPP_{climatic}$). $GPP_{baseline}$ is calculated as the mean GPP over the first two years in the considered time series. The relative change of GPP in response to CO_2 (*i.e.,* β) is derived as the trend of the linear-fit between CO_2 concentration and $GPP_{residual}$ in relative to $GPP_{baseline}$. Similarly, the sensitivity of GPP to temperature (*i.e.,* γ) is derived as the trend of linear-fit between temperature and $GPP_{climatic}$ in relative to $GPP_{baseline}$:

$$\beta = \frac{\frac{\Delta GPP_{residual}}{GPP_{baseline}}}{\Delta CO_2} \times 100\% \quad (3)$$

$$\gamma = \frac{\frac{\Delta GPP_{climatic}}{GPP_{baseline}}}{\Delta Temp} \times 100\% \quad (4)$$

The advantage of the *GPP residual method* is that we separate the confounding factors at different time scales, thus, it can solve the issue of multicollinearity to some extent, when the independent variables are highly correlated to one another. To show the different results yield from the *GPP residual method* and a multivariate regression method, we adopt a simple multivariate regression model as the following:

$$\frac{GPP}{GPP_{baseline}} * 100\% = \beta \times CO_2 + \gamma \times Temp + \rho_{VPD} \times VPD + \rho_{WAI} \times WAI + \rho_{GDD} \times GDD + \rho_{SW_{in}} \times SW_{in} \quad (5)$$

Where β is the sensitivity of GPP to CO_2, and γ is the sensitivity of GPP to temperature. After obtaining β values for each site-month, we calculate the median β. This approach helps to mitigate the influence of outliers. We further estimate the uncertainty of the median β using the bootstrap method. By repeatedly sampling from the considered β distribution, we create multiple bootstrap samples. Each sample is then used to calculate the median β. The standard deviation across these bootstrap estimates provides an estimate of the uncertainty associated with median β. We calculate the median γ and its uncertainty in the same way.

To consider the seasonal and spatial variation of GPP, we further calculate annual β and γ by aggregating monthly β and γ weighted by monthly $GPP_{baseline}$:

$$Annual\ \beta = \sum_{i=1}^{n} \beta_{month_i} \times \frac{GPP_{baseline_i}}{GPP_{gs}} \quad (6)$$

Where i represents a specific month, and n is the total number of months. GPP_{gs} is the sum of baseline GPP across the considered growing season. Similarly, the annual β and γ at each site can be further aggregated across space:

$$mean\ \beta = \sum_{i=1}^{n} Annual\ \beta_i \times \frac{GPP_{gs_i}}{GPP_{sum}} \quad (8)$$

$$mean\ \gamma = \sum_{i=1}^{n} Annual\ \gamma_i \times \frac{GPP_{gs_i}}{GPP_{sum}} \quad (9)$$

Where i represents a specific site, and n is the total number of sites. GPP_{sum} is the sum of baseline GPP across all sites. To assess the robustness of the median β or γ values and determine if they are influenced by site selection, we compare the mean β or γ calculated across all sites, weighted by baseline GPP, with the median β or γ derived from the distribution of monthly β or γ values. If the median value remains relatively stable and comparable to the mean value across all sites, it suggests that the selection of sites does not significantly impact the robustness of the

median β or γ estimations.

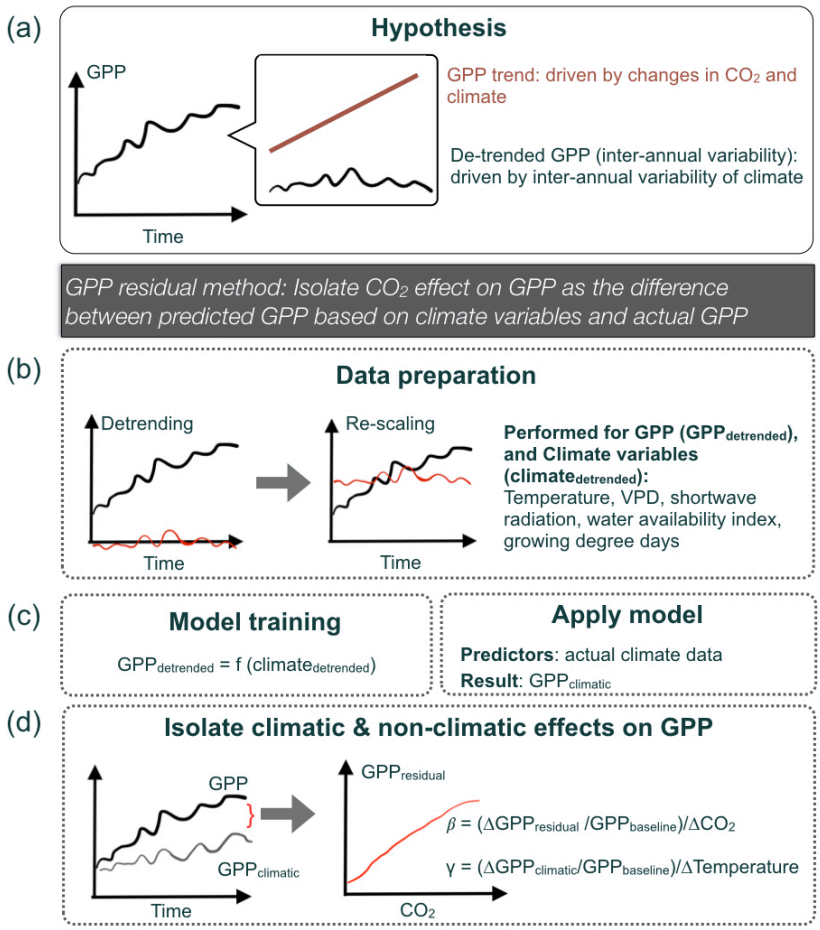

Figure 1. Schematic of the statistical *GPP residual method* to isolate the CO_2 fertilization effect and climatic effect in observational data of GPP. (a) Hypothesis. The overall goal of the *GPP residual method* is to isolate the CO_2 fertilization effect on GPP by removing long-term climate effects inferred from short-term variability. (b) Data preparation. All the time series of climate variables and GPP are detrended and individually rescaled to the long-term mean of each variable. The black lines denote the actual time series for each variable, and the red line denotes the detrended time series. (c) A random forest model or multivariate linear regression model is trained to learn the sensitivity of GPP to the climate variables based on the detrended time series, i.e., interannual variability. (d) The trained model predicts the long-term changes in GPP caused by climate changes using the original time series of climate predictors, including the long-term trend. The non-climate-induced effect on GPP is therefore estimated from the residual of absolute GPP minus climate-induced GPP, shown as the red line.

The EC technique allows for direct measurement of NEE, which is the difference between GPP and ecosystem respiration (RECO):

$$NEE = RECO - GPP \quad (10)$$

The maximum net ecosystem production (NEP_{max}) is defined as the negative sign of the minimum NEE during a day from half-hourly measurement:

$$NEP_{max} = -NEE_{min} \quad (11)$$

In addition to GPP, we further estimate β or γ for NEP_{max} following the same method.

2.3 Validate the *GPP residual method* with a land surface model

We use the terrestrial biosphere model QUINCY (QUantifying Interactions between terrestrial Nutrient CYcles and the climate system; Thum et al., 2019), which has been evaluated against a subset of FLUXNET sites across large geographical ranges and different ecosystem types, to validate the *GPP residual method*. We perform two simulations with identical climate but varying CO_2 concentrations (transient CO_2 as observed, and constant CO_2 at levels of the year 1988) at 166 forested sites distributed across the globe. The model setup and model simulations are identical with the "freeze-CO_2 experiment" in Zhan et al. (2022). For better comparison with eddy covariance records, we take the last twenty years (1999-2018) in the simulations as the time period of the validation.

The advantage of this method is that we can compare the β estimated by the *GPP residual method* ($\beta_{\text{estimated}}$) with β modeled by QUINCY (β_{QUINCY}), which is regarded as a surrogate truth that represents theory of photosynthetic responses to CO_2, climate and water availability. β_{QUINCY} is calculated as the sensitivity of the CO_2-induced change in GPP to CO_2 concentration, in which GPP is calculated as the difference between simulations forced with transient CO_2 and constant CO_2 during the considered time period. β is calculated for each site and each month-of-year. The selection of months follows the same rule as the data preparation in the previous section. $\beta_{\text{estimated}}$ is calculated using the *GPP residual method* elaborated in the previous section from the simulation forced with transient CO_2.

We evaluate the agreement of $\beta_{\text{estimated}}$ and β_{QUINCY} for each forested site (166 sites in total) in the model. We use the root-mean-square error (RMSE) to measure the difference between $\beta_{\text{estimated}}$ and β_{QUINCY} across the growing season. The RMSE of β estimation per site is calculated as:

$$RMSE(\beta) = \sqrt{\frac{\sum_{i=1}^{n}\left(\beta_{estimated_i} - \beta_{QUINCY_i}\right)^2}{n}} \quad (10)$$

where n is the number of months when β is estimated; $\beta_{estimated_i}$ and β_{QUINCY_i} is the β estimated and modeled at month i, respectively. In this study, we use the validated *GPP residual method* to estimate β in tree-dominated ecosystems based on measured meteorological data and the CO_2 atmospheric inversion product.

2.4 β and γ determined from the TRENDY v9 ensemble

We use simulations from twelve process-based global dynamic vegetation models (DGVM) within the TRENDY projects (Sitch et al., 2015; Le Quéré et al., 2018) to derive the modeled β and γ. We use four simulations (called S0, S1, S2, S3 in the TRENDY v9 protocol; see Table S3) with and without land use and land cover changes (LULCCs) under both transient (historically observed) and pre-industrial (constant) environmental conditions. CO_2 effect on GPP modeled by TRENDY ($\beta_{S1\text{-}S0}$) is calculated as the difference between output from S1 and S0, to avoid the effect from climate recycling. To test the robustness of the *GPP residual method* and the potential LULCCs effect, we apply the same statistical method (*i.e.,* the *GPP residual method*) on simulations in S2 and S3, respectively. We derive γ from S2 simulations by calculating the sensitivity of GPP in S2 to temperature. We select grid-cells containing the 38 considered eddy covariance sites in all models. β and γ is calculated for the same site-months as data analyzed in EC records.

3 Results and Discussion

3.1 Evaluating the *GPP residual method* with a land surface model

We develop and test the *GPP residual method* with QUINCY model simulations (Methods) from which we cannot only infer β with our method, but also directly compare with the modeled β. Overall, we find that our method can satisfactorily estimate β, and can capture the seasonal variations of β across biomes. We find β in tropical forest is overall well reproduced by our statistical method, supported by a mean root-mean-square error (RMSE) of 1.2 $gC/m^2/year/ppm$. However, the performance in the cold northern high latitude regions, where part of the boreal

needle leaf forests and temperate forests are located, is slightly diminished, with a mean RMSE of 1.5 gC/m^2/year/ppm (Figure 2a, b). The *GPP residual method* with implemented random forests exhibits better estimation in temperate broadleaf summergreen trees (TeBS), compared with both multivariate regression methods that estimate negative β in TeBS during the beginning and the late growing season (Figure S1, S2). Additionally, we find a slight overestimation accompanied with higher RMSE, during summer months in boreal needleleaf evergreen (BNE) forested sites and boreal needleleaf summergreen (BNS) forested sites. The discrepancy between estimated β and modeled β can be attributed to the limitations associated with constructing a statistical model to estimate the sensitivity of GPP to climate variables relying on interannual variabilities. This means this statistical model does not account for vegetation acclimation on climatic variability in the long-term, such as phenological changes, which cannot be learned from interannual variabilities. Thus, the statistical method exhibits decreased accuracy, particularly in ecosystems where seasonality exerts strong control.

In addition to the limitation of capturing vegetation phenology, we individually consider the effect of rising CO_2 and the effect of changing climatic conditions. Thus, the synergetic effect of rising CO_2 and temperature (Drake et al., 1997) is not considered in our approach, where *e.g., increasing CO_2 can modify plants' response to temperature*. This simplification could result in the overestimation of the CO_2 fertilization effect on GPP. On the other hand, the anomalies associated with extreme events can be theoretically reproduced by the statistical method. However, given that only a few instances of extreme events are in the training dataset, we acknowledge that the non-linear relationship between climate and GPP during extreme conditions can induce errors in the estimation of β. Overall, we find encouraging consistency between the β estimated by the *GPP residual method* and β modeled by QUINCY.

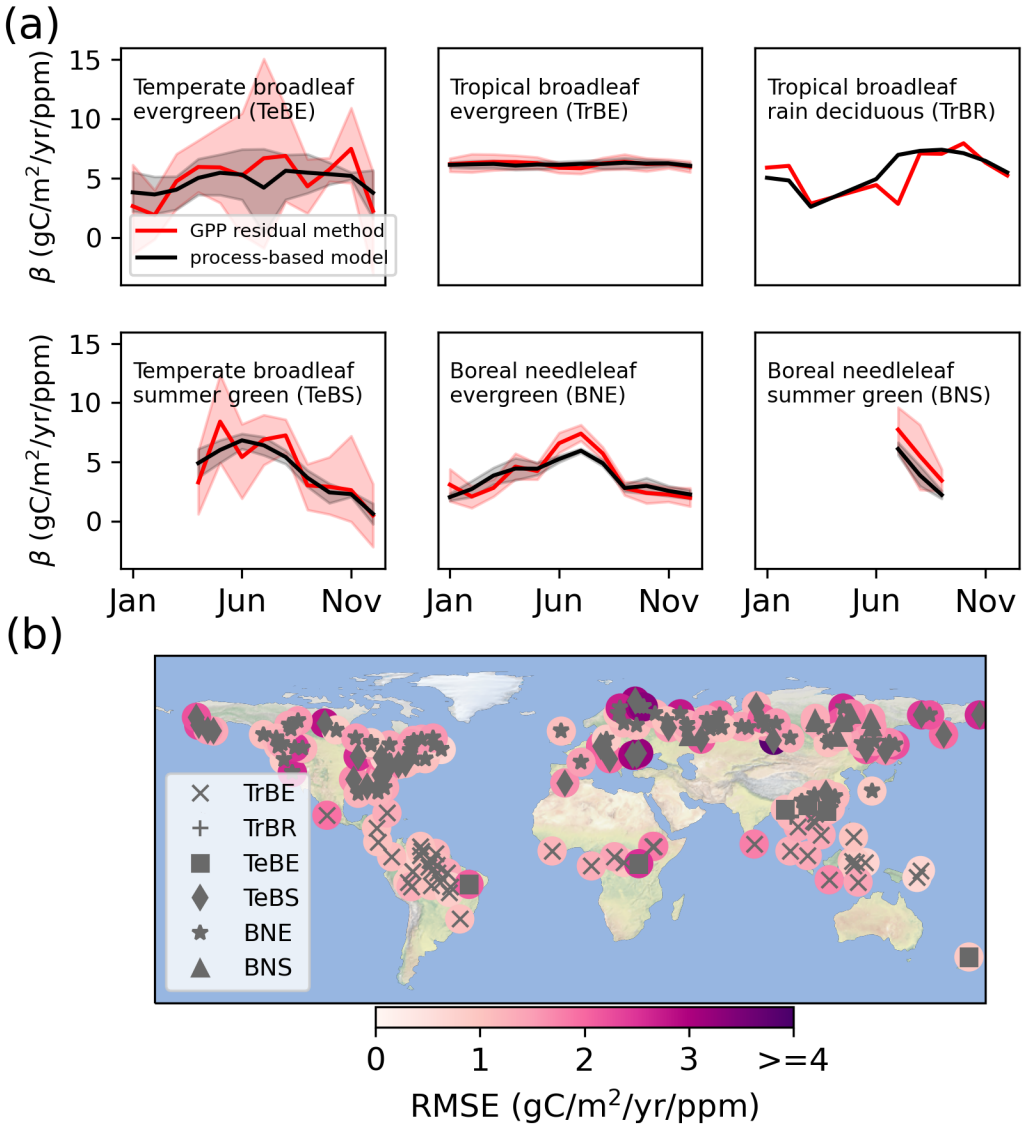

308

309 **Figure 2.** Validation of the *GPP residual method* with QUINCY model simulations. (a) Seasonal
310 variation of β across vegetation types estimated by the *GPP residual method* with a random
311 forest model in red and QUINCY in black (166 sites with 1220 site-months). The red and black
312 shaded area depicts one standard deviation around the mean value of β across multiple site-
313 months (solid lines). (b) The map shows the root mean square error (RMSE) between estimated
314 β and modeled β in the growing season for each site in the QUINCY model. Brighter color
315 indicates lower bias and thus a better performance of the *GPP residual method*.

316 3.2 CO_2 fertilization effect in forested ecosystems inferred from eddy covariance records

317 Using the *GPP residual method*, we estimate the strength of the CO_2 fertilization effect on

photosynthetic carbon uptake as recorded in eddy covariance (EC) time series at 38 forested sites (Figure 3). We assess the sensitivity of GPP to CO_2, denoted β (Methods), separately for each individual month across the years of the time series to account for seasonal variations. The median β value across all sites and months is 16.4 ± 4.1 % increase in GPP per 100 ppm rise in atmospheric CO_2. While β displays considerable variability across sites and months, positive β values are consistently observed in 61 % of sites for at least two months in the record. The strongest enhancement of β occurs during the boreal summer months, although a selection of sites exhibits stronger effects in spring (*e.g., CA-Ca3, IT-Ren*) or autumn (*e.g., US-GLE, FR-FBn*).

Among the analyzed sites, the top seven sites listed in Figure 3a (DE-Hzd, CA-LP1, CA-Ca3, CA-Cbo, US-GLE, IT-Ren, CA-TP4) exhibit the most pronounced GPP enhancement, with their site-specific annual mean β values surpassing the top 20% of all the sites. In addition to the median β value across all sites and months, we aggregate monthly β based on the monthly baseline GPP, to represent the mean β across selected sites. The aggregated mean β is 14.9 % per 100 ppm, indicating the median β is representative and not biased by the site selection, considering the variation in GPP across sites.

The presented approach lacks the ability to isolate additional hidden long-term effects stemming from human activities, and these effects may manifest in an over- or under-estimation of β derived at individual sites. Notably, certain sites (*e.g., DE-Obe, CH-Dav, FI-Let, DE-Hai*) exhibit negative β values consistently throughout the growing months. The negative β identified at the "CH-Dav" site may be associated with a disturbance event, specifically a harvest conducted in the year 2006. Similarly, the thinning activity at the "FI-Let" site in 2016 induced a declining of GPP trend, leading to a negative β estimate throughout the year. Forest in the "DE-Hai" site is recoving from a sever drought. Conversely, other drivers such as nitrogen deposition at nitrogen-limited sites (De Vries et al., 2006; Sutton et al., 2008; de Vries et al., 2014) or forests undergoing succession (Pugh et al., 2019) can induce a long-term increase of GPP, potentially resulting in an overestimation of β. However, these rather site-specific trends in opposing directions may offset each other within a well-distributed and sufficiently large sample size, enabling the median β across sites to predominantly capture the widespread CO_2 fertilization effect. This notion is supported by excluding known disturbance sites (*e.g., forest*

thinning) from the analysis, resulting in a median β (11.9 ± 4.1 % per 100 ppm) that does not significantly differ from the β estimated using all sites (Figure 3b).

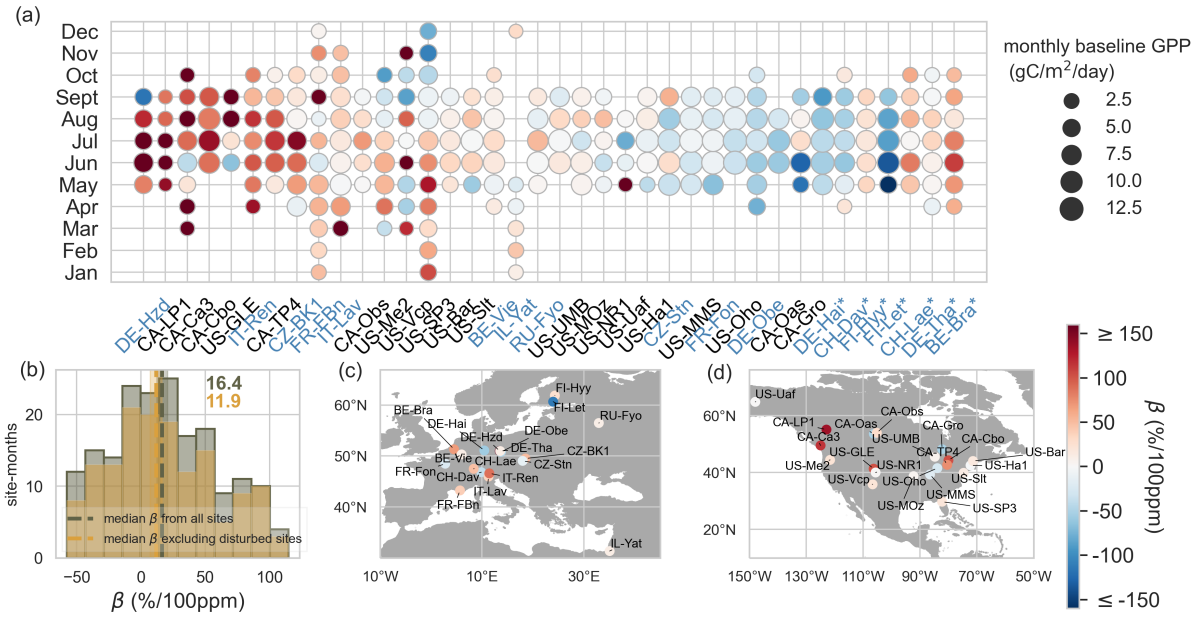

Figure 3. Estimation of β from eddy covariance data using the *GPP residual method* with a random forest model. (a) Plot showing the estimated β for each eddy covariance site across months in the growing season. The size of circles represents the magnitude of monthly baseline GPP. Sites are shown in descending order of the annual mean β (Methods). Site-codes marked by a star are presented separately at the end of the list, indicating that disturbances have been recorded at those specific sites. Site-codes shown in blue and black color locate in Europe (c) and North America (d). (b) The histogram of β values shown in panel (a). The grey (yellow) vertical dashed lines denote the median β (Methods) estimated from all sites and months (excluding the disturbed sites). The grey (yellow) shaded area indicates the bootstrap estimates for the uncertainty of median β from all sites (excluding the disturbed sites). Maps (c) and (d) display the annual mean β values at each site.

The daily maximum net ecosystem production (NEP_{max}) provides insights into the peak photosynthetic activity of the ecosystem during optimal conditions within a day. It is valuable for understanding the ecosystem's contribution to carbon sequestration. In addition to GPP, we identify the CO_2 fertilization effect on NEP_{max} as 17.2 ± 3.6 % per 100 ppm (Figure 4). The temporal and spatial variation of β in NEP_{max} is consistent with β in GPP (Figure 3), adding additional observational evidence of the CO_2 fertilization effect for better understanding of the global carbon cycle dynamics.

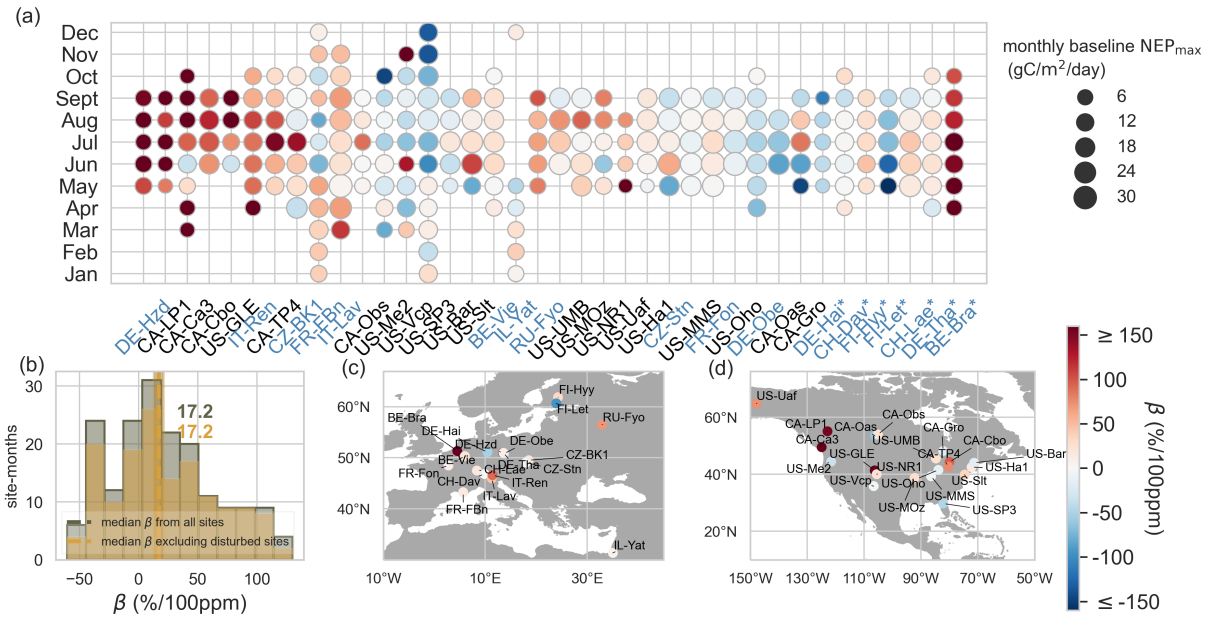

Figure 4. Estimation of β from eddy covariance data using the *GPP residual method* with a random forest model. Analogous to Figure 3 but β is estimated for NEP_{max}.

Next, we assess the robustness of our findings by testing multiple regression methods in estimating the GPP sensitivity to climatic changes, and evaluate their statistical performance. Testing a multivariate linear regression instead of a random forest regressor, we find that the median β yields a slightly different estimate of 15.1 ± 5.0 % per 100 ppm (Figure S3). If we however apply the multivariate regression model without accounting for confounding drivers of rising CO_2 and climatic changes (Methods), the median β is notably lower and amounts to 11.4 ± 5.6 % per 100 ppm (Figure. S4). We utilize the "Out-of-Bag" (OOB) score to estimate the performance of the random forest regressor on unseen data without the need for a separate validation set (Methods). Although there are instances of relatively low OOB score at certain sites and months, no clear relationship emerges between estimated β values and model performances (Figure S5).

3.3 Exploring the spatial variation of the CO_2 fertilization effect

We further explore the spatial variability in estimated β. Thereby, we assess the roles of plant functional types (PFTs), forest age, temperature, VPD and maximum leaf area index (LAI). Past studies have found stronger stomatal responsiveness to changes in CO_2 in deciduous trees versus conifers (Saxe et al., 1998; Medlyn et al., 2001; Brodribb et al., 2009; Klein and Ramon, 2019),

388 although variability exists when assessing their different responses in photosynthesis (Saxe et al.,
389 1998). Overall, we find a greater enhancement in GPP in evergreen needle-leaved forest (ENF)
390 in response to increasing CO_2 (Figure S6), compared with deciduous broadleaf forest (DBF). The
391 difference in GPP responses to increasing CO_2 across PFTs may vary with scales, or complex
392 environmental conditions (*e.g., under stress or not*). Future work may focus on this difference in
393 more detail. An open question is whether mature forests, which may be approaching a quasi-
394 equilibrium state, are responding to CO_2 and climate in the same fashion as younger stands (Kira
395 and Shidei, 1967; Odum, 1969; Luyssaert et al., 2008). We find no significant relationship
396 between β and forest age, but we show a tendency of GPP enhancement to decline towards older
397 stands (Figure S7a). Theoretically, the enhancement in GPP would relate to differences in
398 growing season temperature and VPD, with greater enhancement at warmer growth temperatures
399 (suppression of photorespiration; Baig et al., 2015). However, we find no significant but slight
400 negative trend in the relationship between β and temperature as well as VPD (Figure S7b, c).
401 This trend may be attributed to the combined impact of temperature and VPD. We find a positive
402 tendency of β with increasing site maximum LAI (Figure S7d), which could be an interaction
403 between rising CO_2 and exponential growth phase (*i.e., regrowth*).

404 3.4 Comparing the CO_2 fertilization effect inferred from eddy covariance sites and TRENDY
405 ensemble

406 We compare our EC based β estimates with an ensemble of twelve process-based global
407 dynamic vegetation models (DGVM) following the TRENDY simulation protocol (Sitch et al.,
408 2015; Le Quéré et al., 2018). The TRENDY ensemble consists of four experiments (Table S3):
409 the pre-industrial control run (S0), the run considering only CO_2 changes (S1), the run
410 considering CO_2 and climate change forcings (S2), and the latter with additional prescribed land-
411 use and land-cover changes (S3). To conduct the comparison, we extract model time series from
412 the individual grid-cells containing the 38 considered eddy-covariance sites. The modeled CO_2
413 fertilization effect inferred by calculating the difference $\beta_{S1\text{-}S0}$, exhibits a large spread among the
414 TRENDY models. The median $\beta_{S1\text{-}S0}$ across the grid-cells and models is 17.7 % per 100 ppm,
415 which is remarkably close to the median β obtained through the *GPP residual method* using EC
416 records. Seven models (VISIT, CLM5.0, JULES-ES-1p0, CLASSIC, ISAM, ORCHIDEE and
417 LPJ-GUESS) fall within the bootstrapped uncertainty range of the median β estimated from

observations (Figure 5; Methods). We acknowledge the limitation of this comparison, as it involves contrasting site-level estimates with grid-level results, which is influenced by the heterogeneity within each grid-cell. Nevertheless, we argue that the median values across the sites and grid-cells provide a more aggregated perspective that helps mitigate the influence of sub-grid heterogeneity.

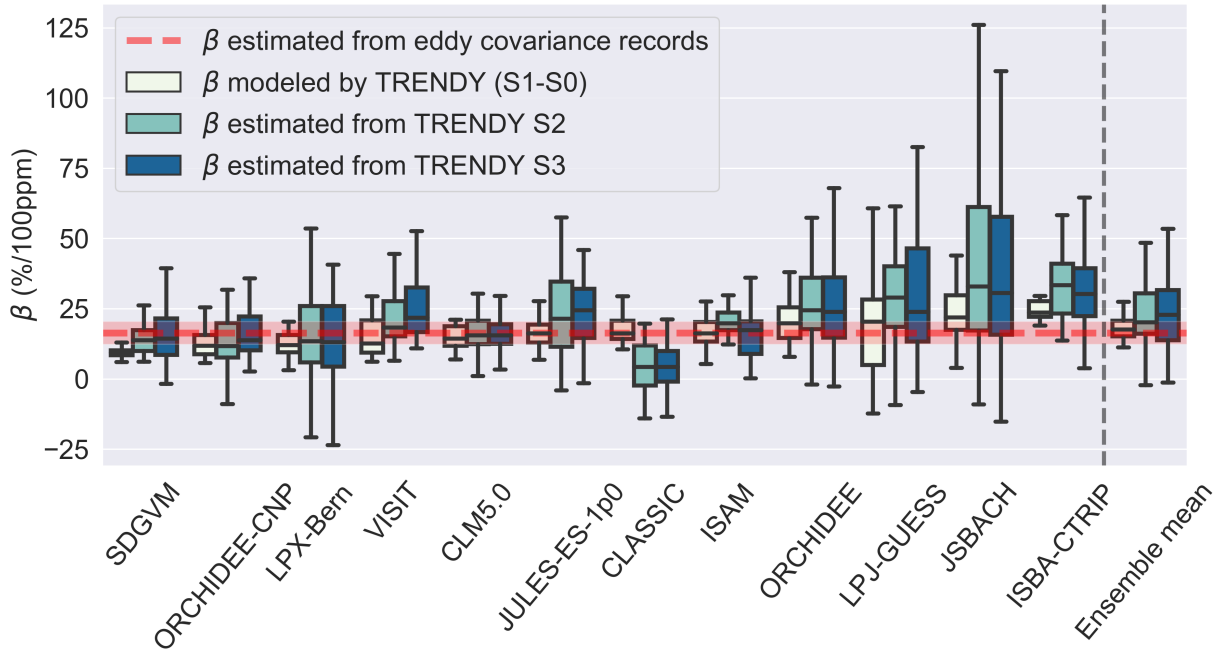

Figure 5. Comparing β estimated from eddy covariance data and the TRENDY model ensemble. The medians and interquartile ranges of β are shown for each model and for the ensemble mean, as horizontal lines within the boxes, and the upper and bottom lines of the box, respectively. Each box includes grid-cells containing the 38 considered eddy covariance sites. Box plots for individual models are in an ascending order based to the median β. The dotted red line represents the median β derived from eddy covariance records (as shown also in Figure 3), with the uncertainty showing in shaded area.

Other factors, such as nitrogen deposition, disturbances, and particularly land management, can influence ecosystem productivity as recorded in EC data. These factors potentially influence the estimation of β using the *GPP residual method*. To assess the effect of land-use and land-cover changes (LULCCs) on β estimation, we compare β derived from the TRENDY S2 and S3 simulations using the *GPP residual method*. With the exception of the LPJ-GUESS and JULES-ES-1p0 models, the ensemble mean of β_{S2} closely aligns with β_{S3} (Figure 5), suggesting that the neglected effects of LULCCs do not substantially affect the β estimation. Furthermore, in line

with the validation using QUINCY simulations, the *GPP residual method* tends to slightly overestimate β when comparing β_{S2} with $\beta_{S1\text{-}S0}$ derived from TRENDY. This further emphasizes that the method cannot account for long-term vegetation acclimation and phenological changes; however, these effects are minor within the considered time period.

3.5 Influence of climatic changes on productivity throughout the season

Conventionally, the γ factor is defined as the sensitivity of land carbon storage to climate variations using temperature change as the proxy (Friedlingstein et al., 2006; Gregory et al., 2009; Arora et al., 2020). Analogously, we define γ as the relative change in the climate-driven GPP component over temperature change, which is already obtained in the *GPP residual method* (Methods). The median γ in GPP estimated from the EC dataset is 1.8 ± 0.2 % per Kelvin (Figure 5). Comparing this to the sensitivity of GPP to CO_2, assuming a 100 pm increase in atmospheric CO_2 concentration is roughly equivalent to 1 Kelvin temperature increase in the historical period, we find that γ is considerably lower than β, in line with previous studies (Fernández-Martínez et al., 2017; Chen et al., 2022). The median γ in NEP_{max} (-0.2 ± 0.2 % per Kelvin) is much lower than γ in GPP, reflecting a negative response of NEP_{max} to temperature variations, particularly at the peak of the growing season (Figure S8). The median γ estimated from the TRENDY ensemble (S2 simulations) is 0.8 ± 0.2 % per Kelvin (Figure S9). Also, γ exhibits a large spread among models compared to γ from EC, suggesting a more pronounced uncertainty in the process representation in estimating ecosystem responses to climate changes among the land-surface models (Figure S10). A clear seasonality of γ emerges in both observations and models (Figure 5, Figure S8, Figure S9). While γ is higher at the beginning and the end of the growing season for most of the sites, most sites show negative γ in at least one month of the growing season (26 out of 38 in the EC estimated GPP; 36 out of 38 in the EC measured NEP_{max}; 33 out of 38 in the TRENDY ensemble mean). Our results indicate that warming may have a positive effect on vegetation productivity at colder conditions and a potential negative effect in warm climate. A high temperature is usually accompanied by a high VPD, which limits the stomatal conductance and evapotranspiration (Park Williams et al., 2013; Novick et al., 2016). On the other hand, plant productivity response to temperature is associated with water availability; a positive effect of temperature can occur when water is not limiting the ecosystem functioning (Fernández-Martínez et al., 2019). Additionally, the negative climate-

carbon feedback may contribute to, and potentially partly mask or enhance the CO_2 fertilization effect.

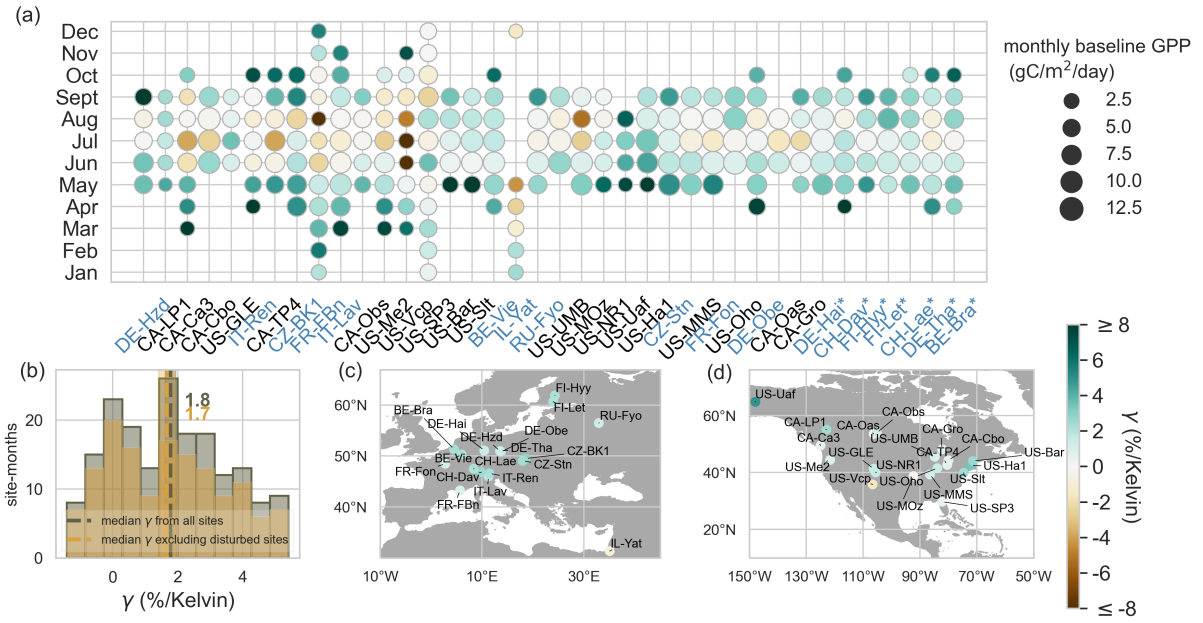

Figure 6. Estimation of γ from eddy covariance dataset using the *GPP residual method* with a random forest model. (a) Plot showing the estimated γ for each eddy covariance site across months in the growing season. The size of circles represents the magnitude of monthly baseline GPP. Sites are shown in descending order of the annual mean γ (Methods). Site-codes marked by a star are presented separately at the end of the list, indicating that disturbances have been recorded at those specific sites. Site-codes shown in blue and black color locate in Europe (c) and North America (d). (b) The histogram of γ values shown in panel (a). The grey (yellow) vertical dashed lines denote the median γ (Methods) estimated from all sites and months (excluding the disturbed sites). The grey (yellow) shaded area indicates the bootstrap estimates for the uncertainty of median γ from all sites (excluding the disturbed sites). Maps (c) and (d) display the annual mean γ values at each site.

Overall, we recognize the inherent limitations in EC-based data acquisition, the assumptions of the *GPP residual method*, and the potential influence of other long-term factors such as human activities, which can introduce biases in the estimation of β and γ from observations. However, despite these challenges, the β and γ values estimated from the EC records align with the β and γ values simulated by the TRENDY model, both in terms of the median values across multiple sites and the seasonality of γ. Furthermore, utilizing the TRENDY simulations, we demonstrate that the discrepancy in β estimation, influenced by land use and land cover changes, remains within an acceptable range.

4 Conclusions

Our study isolates a robust, multi-decadal enhancement in vegetation productivity ($\boldsymbol{\beta_{GPP}}$ = 16.4 ± 4 % per 100 ppm, $\boldsymbol{\beta_{NEP_{max}}}$ = 17.2 ± 4 % per 100 ppm) across Northern Hemisphere forests in response to the rising atmospheric CO_2 concentration. We further diagnose the median value of GPP sensitivity to temperature (γ) of 1.8 ± 0.2 % per Kelvin, and find evidence of a negative effect of temperature on photosynthesis at the peak of the growing season. Assuming a 100 pm increase in CO_2 concentration is equivalent to 1 Kelvin temperature increase, the negative temperature effect potentially masks the positive increasing CO_2 effect on GPP. While the TRENDY ensemble captures the median β and γ inferred from eddy covariance records, there is a notable variation in β and γ exhibited between individual models. To improve the representation of the temperature effect on GPP in TRENDY models, further studies should focus on reducing uncertainties associated with physiological processes and incorporating multi-model constraints. This study paves the way for future investigations into long-term drivers of change and ecosystem functioning. We anticipate that our approach could be readily applied to other ecosystems (*e.g., drylands*), other datasets (long-term satellite records of change, *i.e., vegetation greenness, etc.*), and other variables that describe ecosystem function (*e.g., evapotranspiration*). Together with a wide range of evidence of global vegetation productivity in response to rising atmospheric CO_2 concentration and climate change, a better estimation of the remaining carbon budget to achieve the climate goals in the Paris Agreement is possible.

Acknowledgments

Chunhui Zhan is supported by the International Max Planck Research School (IMPRS). Markus Reichstein and Alexander J. Winkler acknowledge the support by the European Research Council (ERC) Synergy Grant "Understanding and Modelling the Earth System with Machine Learning (USMILE)" under the Horizon 2020 research and innovation programm (grant agreement number 855187). René Orth is supported by the German Research Foundation (Emmy Noether grant number 391059971). Sönke Zaehle is supported by the European Research Council (ERC) under the European Union's Horizon 2020 research and innovation programm (QUINCY; grant number 647204). Martin De Kauwe acknowledges funding from the UK Natural Environment Research Council (NE/W010003/1). Hui Yang is supported by the Project Office BIOMASS (grant number 50EE1904) funded by the German Federal Ministry of

Economics and Technology. Chunhui Zhan thanks Xin Yu, Martin Jung, Mirco Migliavacca, Ulisse Gomarasca for their insights of using FLUXNET data, and Nuno Carvalhais for valuable discussion. This work used eddy covariance data acquired and shared by the FLUXNET community, including ICOS and AmeriFlux.

Open Research

The observational data that support the findings of this study are available in the ICOS warm winter 2020 product (https://www.icos-cp.eu/data-products/2G60-ZHAK) and Ameriflux (https://ameriflux.lbl.gov/).

The codes are available online: https://doi.org/10.5281/zenodo.10125474.

References

Aragão, L.E.O.C., Malhi, Y., Roman-Cuesta, R.M., Saatchi, S., Anderson, L.O., Shimabukuro, Y.E., 2007. Spatial patterns and fire response of recent Amazonian droughts. Geophys. Res. Lett. 34. https://doi.org/10.1029/2006GL028946

Arora, V.K., Katavouta, A., Williams, R.G., Jones, C.D., Brovkin, V., Friedlingstein, P., Schwinger, J., Bopp, L., Boucher, O., Cadule, P., Chamberlain, M.A., Christian, J.R., Delire, C., Fisher, R.A., Hajima, T., Ilyina, T., Joetzjer, E., Kawamiya, M., Koven, C.D., Krasting, J.P., Law, R.M., Lawrence, D.M., Lenton, A., Lindsay, K., Pongratz, J., Raddatz, T., Séférian, R., Tachiiri, K., Tjiputra, J.F., Wiltshire, A., Wu, T., Ziehn, T., 2020. Carbon–concentration and carbon–climate feedbacks in CMIP6 models and their comparison to CMIP5 models. Biogeosciences 17, 4173–4222. https://doi.org/10.5194/bg-17-4173-2020

Baig, S., Medlyn, B.E., Mercado, L.M., Zaehle, S., 2015. Does the growth response of woody plants to elevated CO2 increase with temperature? A model-oriented meta-analysis. Glob. Change Biol. 21, 4303–4319. https://doi.org/10.1111/gcb.12962

Baldocchi, D.D., 2020. How eddy covariance flux measurements have contributed to our understanding of Global Change Biology. Glob. Change Biol. 26, 242–260. https://doi.org/10.1111/gcb.14807

Besnard, S., Carvalhais, N., Arain, M.A., Black, A., de Bruin, S., Buchmann, N., Cescatti, A., Chen, J., Clevers, J.G.P.W., Desai, A.R., Gough, C.M., Havrankova, K., Herold, M., Hörtnagl, L., Jung, M., Knohl, A., Kruijt, B., Krupkova, L., Law, B.E., Lindroth, A., Noormets, A., Roupsard, O., Steinbrecher, R., Varlagin, A., Vincke, C., Reichstein, M.,

2018. Quantifying the effect of forest age in annual net forest carbon balance. Environ. Res. Lett. 13, 124018. https://doi.org/10.1088/1748-9326/aaeaeb

Brodribb, T.J., McAdam, S.A.M., Jordan, G.J., Feild, T.S., 2009. Evolution of stomatal responsiveness to CO2 and optimization of water-use efficiency among land plants. New Phytol. 183, 839–847. https://doi.org/10.1111/j.1469-8137.2009.02844.x

Campbell, J.E., Berry, J.A., Seibt, U., Smith, S.J., Montzka, S.A., Launois, T., Belviso, S., Bopp, L., Laine, M., 2017. Large historical growth in global terrestrial gross primary production. Nature 544, 84–87. https://doi.org/10.1038/nature22030

Chen, C., Riley, W.J., Prentice, I.C., Keenan, T.F., 2022. CO2 fertilization of terrestrial photosynthesis inferred from site to global scales. Proc. Natl. Acad. Sci. 119, e2115627119. https://doi.org/10.1073/pnas.2115627119

Chevallier, F., Ciais, P., Conway, T.J., Aalto, T., Anderson, B.E., Bousquet, P., Brunke, E.G., Ciattaglia, L., Esaki, Y., Fröhlich, M., Gomez, A., Gomez-Pelaez, A.J., Haszpra, L., Krummel, P.B., Langenfelds, R.L., Leuenberger, M., Machida, T., Maignan, F., Matsueda, H., Morguí, J.A., Mukai, H., Nakazawa, T., Peylin, P., Ramonet, M., Rivier, L., Sawa, Y., Schmidt, M., Steele, L.P., Vay, S.A., Vermeulen, A.T., Wofsy, S., Worthy, D., 2010. CO2 surface fluxes at grid point scale estimated from a global 21 year reanalysis of atmospheric measurements. J. Geophys. Res. Atmospheres 115. https://doi.org/10.1029/2010JD013887

Chevallier, F., Fisher, M., Peylin, P., Serrar, S., Bousquet, P., Bréon, F.-M., Chédin, A., Ciais, P., 2005. Inferring CO2 sources and sinks from satellite observations: Method and application to TOVS data. J. Geophys. Res. Atmospheres 110. https://doi.org/10.1029/2005JD006390

De Kauwe, M.G., Medlyn, B.E., Zaehle, S., Walker, A.P., Dietze, M.C., Hickler, T., Jain, A.K., Luo, Y., Parton, W.J., Prentice, I.C., Smith, B., Thornton, P.E., Wang, S., Wang, Y.-P., Wårlind, D., Weng, E., Crous, K.Y., Ellsworth, D.S., Hanson, P.J., Seok Kim, H.-, Warren, J.M., Oren, R., Norby, R.J., 2013. Forest water use and water use efficiency at elevated CO2: a model-data intercomparison at two contrasting temperate forest FACE sites. Glob. Change Biol. 19, 1759–1779. https://doi.org/10.1111/gcb.12164

de Vries, W., Du, E., Butterbach-Bahl, K., 2014. Short and long-term impacts of nitrogen deposition on carbon sequestration by forest ecosystems. Curr. Opin. Environ. Sustain.,

582 SI: System dynamics and sustainability 9–10, 90–104.
583 https://doi.org/10.1016/j.cosust.2014.09.001
584 De Vries, W., Reinds, G.J., Gundersen, P., Sterba, H., 2006. The impact of nitrogen deposition
585 on carbon sequestration in European forests and forest soils. Glob. Change Biol. 12,
586 1151–1173. https://doi.org/10.1111/j.1365-2486.2006.01151.x
587 Drake, B.G., Gonzàlez-Meler, M.A., Long, S.P., 1997. MORE EFFICIENT PLANTS: A
588 Consequence of Rising Atmospheric CO2? Annu. Rev. Plant Physiol. Plant Mol. Biol.
589 48, 609–639. https://doi.org/10.1146/annurev.arplant.48.1.609
590 Ehlers, I., Augusti, A., Betson, T.R., Nilsson, M.B., Marshall, J.D., Schleucher, J., 2015.
591 Detecting long-term metabolic shifts using isotopomers: CO2-driven suppression of
592 photorespiration in C3 plants over the 20th century. Proc. Natl. Acad. Sci. 112, 15585–
593 15590. https://doi.org/10.1073/pnas.1504493112
594 Fernández-Martínez, M., Sardans, J., Chevallier, F., Ciais, P., Obersteiner, M., Vicca, S.,
595 Canadell, J.G., Bastos, A., Friedlingstein, P., Sitch, S., Piao, S.L., Janssens, I.A.,
596 Peñuelas, J., 2019. Global trends in carbon sinks and their relationships with CO2 and
597 temperature. Nat. Clim. Change 9, 73–79. https://doi.org/10.1038/s41558-018-0367-7
598 Fernández-Martínez, M., Vicca, S., Janssens, I.A., Ciais, P., Obersteiner, M., Bartrons, M.,
599 Sardans, J., Verger, A., Canadell, J.G., Chevallier, F., Wang, X., Bernhofer, C., Curtis,
600 P.S., Gianelle, D., Grünwald, T., Heinesch, B., Ibrom, A., Knohl, A., Laurila, T., Law,
601 B.E., Limousin, J.M., Longdoz, B., Loustau, D., Mammarella, I., Matteucci, G., Monson,
602 R.K., Montagnani, L., Moors, E.J., Munger, J.W., Papale, D., Piao, S.L., Peñuelas, J.,
603 2017. Atmospheric deposition, CO2, and change in the land carbon sink. Sci. Rep. 7,
604 9632. https://doi.org/10.1038/s41598-017-08755-8
605 Flechard, C.R., Ibrom, A., Skiba, U.M., de Vries, W., van Oijen, M., Cameron, D.R., Dise, N.B.,
606 Korhonen, J.F.J., Buchmann, N., Legout, A., Simpson, D., Sanz, M.J., Aubinet, M.,
607 Loustau, D., Montagnani, L., Neirynck, J., Janssens, I.A., Pihlatie, M., Kiese, R.,
608 Siemens, J., Francez, A.-J., Augustin, J., Varlagin, A., Olejnik, J., Juszczak, R., Aurela,
609 M., Berveiller, D., Chojnicki, B.H., Dämmgen, U., Delpierre, N., Djuricic, V., Drewer, J.,
610 Dufrêne, E., Eugster, W., Fauvel, Y., Fowler, D., Frumau, A., Granier, A., Gross, P.,
611 Hamon, Y., Helfter, C., Hensen, A., Horváth, L., Kitzler, B., Kruijt, B., Kutsch, W.L.,
612 Lobo-do-Vale, R., Lohila, A., Longdoz, B., Marek, M.V., Matteucci, G., Mitosinkova,

M., Moreaux, V., Neftel, A., Ourcival, J.-M., Pilegaard, K., Pita, G., Sanz, F., Schjoerring, J.K., Sebastià, M.-T., Tang, Y.S., Uggerud, H., Urbaniak, M., van Dijk, N., Vesala, T., Vidic, S., Vincke, C., Weidinger, T., Zechmeister-Boltenstern, S., Butterbach-Bahl, K., Nemitz, E., Sutton, M.A., 2020. Carbon–nitrogen interactions in European forests and semi-natural vegetation – Part 1: Fluxes and budgets of carbon, nitrogen and greenhouse gases from ecosystem monitoring and modelling. Biogeosciences 17, 1583–1620. https://doi.org/10.5194/bg-17-1583-2020

Friedlingstein, P., Cox, P., Betts, R., Bopp, L., Bloh, W. von, Brovkin, V., Cadule, P., Doney, S., Eby, M., Fung, I., Bala, G., John, J., Jones, C., Joos, F., Kato, T., Kawamiya, M., Knorr, W., Lindsay, K., Matthews, H.D., Raddatz, T., Rayner, P., Reick, C., Roeckner, E., Schnitzler, K.-G., Schnur, R., Strassmann, K., Weaver, A.J., Yoshikawa, C., Zeng, N., 2006. Climate–Carbon Cycle Feedback Analysis: Results from the C4MIP Model Intercomparison. J. Clim. 19, 3337–3353. https://doi.org/10.1175/JCLI3800.1

Gregory, J.M., Jones, C.D., Cadule, P., Friedlingstein, P., 2009. Quantifying Carbon Cycle Feedbacks. J. Clim. 22, 5232–5250. https://doi.org/10.1175/2009JCLI2949.1

Hovenden, M.J., Newton, P.C.D., Wills, K.E., 2014. Seasonal not annual rainfall determines grassland biomass response to carbon dioxide. Nature 511, 583–586. https://doi.org/10.1038/nature13281

Keenan, T.F., Hollinger, D.Y., Bohrer, G., Dragoni, D., Munger, J.W., Schmid, H.P., Richardson, A.D., 2013. Increase in forest water-use efficiency as atmospheric carbon dioxide concentrations rise. Nature 499, 324–327. https://doi.org/10.1038/nature12291

Kira, T., Shidei, T., 1967. Primary Production and Turnover of Organic Matter in Different Forest Ecosystems of the Western Pacific. Jpn. J. Ecol. 17, 70–87. https://doi.org/10.18960/seitai.17.2_70

Klein, T., Ramon, U., 2019. Stomatal sensitivity to CO2 diverges between angiosperm and gymnosperm tree species. Funct. Ecol. 33, 1411–1424. https://doi.org/10.1111/1365-2435.13379

Knauer, J., Zaehle, S., Reichstein, M., Medlyn, B.E., Forkel, M., Hagemann, S., Werner, C., 2017. The response of ecosystem water-use efficiency to rising atmospheric CO_2 concentrations: sensitivity and large-scale biogeochemical implications. New Phytol. 213, 1654–1666. https://doi.org/10.1111/nph.14288

644 Le Quéré, C., Andrew, R.M., Friedlingstein, P., Sitch, S., Pongratz, J., Manning, A.C.,
645 Korsbakken, J.I., Peters, G.P., Canadell, J.G., Jackson, R.B., Boden, T.A., Tans, P.P.,
646 Andrews, O.D., Arora, V.K., Bakker, D.C.E., Barbero, L., Becker, M., Betts, R.A., Bopp,
647 L., Chevallier, F., Chini, L.P., Ciais, P., Cosca, C.E., Cross, J., Currie, K., Gasser, T.,
648 Harris, I., Hauck, J., Haverd, V., Houghton, R.A., Hunt, C.W., Hurtt, G., Ilyina, T., Jain,
649 A.K., Kato, E., Kautz, M., Keeling, R.F., Klein Goldewijk, K., Körtzinger, A.,
650 Landschützer, P., Lefèvre, N., Lenton, A., Lienert, S., Lima, I., Lombardozzi, D., Metzl,
651 N., Millero, F., Monteiro, P.M.S., Munro, D.R., Nabel, J.E.M.S., Nakaoka, S., Nojiri, Y.,
652 Padin, X.A., Peregon, A., Pfeil, B., Pierrot, D., Poulter, B., Rehder, G., Reimer, J.,
653 Rödenbeck, C., Schwinger, J., Séférian, R., Skjelvan, I., Stocker, B.D., Tian, H.,
654 Tilbrook, B., Tubiello, F.N., van der Laan-Luijkx, I.T., van der Werf, G.R., van Heuven,
655 S., Viovy, N., Vuichard, N., Walker, A.P., Watson, A.J., Wiltshire, A.J., Zaehle, S., Zhu,
656 D., 2018. Global Carbon Budget 2017. Earth Syst. Sci. Data 10, 405–448.
657 https://doi.org/10.5194/essd-10-405-2018
658 Luyssaert, S., Schulze, E.-D., Börner, A., Knohl, A., Hessenmöller, D., Law, B.E., Ciais, P.,
659 Grace, J., 2008. Old-growth forests as global carbon sinks. Nature 455, 213–215.
660 https://doi.org/10.1038/nature07276
661 Mastrotheodoros, T., Pappas, C., Molnar, P., Burlando, P., Keenan, T.F., Gentine, P., Gough,
662 C.M., Fatichi, S., 2017. Linking plant functional trait plasticity and the large increase in
663 forest water use efficiency. J. Geophys. Res. Biogeosciences 122, 2393–2408.
664 https://doi.org/10.1002/2017JG003890
665 Medlyn, B.E., Barton, C.V.M., Broadmeadow, M.S.J., Ceulemans, R., De Angelis, P.,
666 Forstreuter, M., Freeman, M., Jackson, S.B., Kellomäki, S., Laitat, E., Rey, A., Roberntz,
667 P., Sigurdsson, B.D., Strassemeyer, J., Wang, K., Curtis, P.S., Jarvis, P.G., 2001.
668 Stomatal conductance of forest species after long-term exposure to elevated CO2
669 concentration: a synthesis. New Phytol. 149, 247–264. https://doi.org/10.1046/j.1469-
670 8137.2001.00028.x
671 Migliavacca, M., Musavi, T., Mahecha, M.D., Nelson, J.A., Knauer, J., Baldocchi, D.D., Perez-
672 Priego, O., Christiansen, R., Peters, J., Anderson, K., Bahn, M., Black, T.A., Blanken,
673 P.D., Bonal, D., Buchmann, N., Caldararu, S., Carrara, A., Carvalhais, N., Cescatti, A.,
674 Chen, J., Cleverly, J., Cremonese, E., Desai, A.R., El-Madany, T.S., Farella, M.M.,

675 Fernández-Martínez, M., Filippa, G., Forkel, M., Galvagno, M., Gomarasca, U., Gough,
676 C.M., Göckede, M., Ibrom, A., Ikawa, H., Janssens, I.A., Jung, M., Kattge, J., Keenan,
677 T.F., Knohl, A., Kobayashi, H., Kraemer, G., Law, B.E., Liddell, M.J., Ma, X.,
678 Mammarella, I., Martini, D., Macfarlane, C., Matteucci, G., Montagnani, L., Pabon-
679 Moreno, D.E., Panigada, C., Papale, D., Pendall, E., Penuelas, J., Phillips, R.P., Reich,
680 P.B., Rossini, M., Rotenberg, E., Scott, R.L., Stahl, C., Weber, U., Wohlfahrt, G., Wolf,
681 S., Wright, I.J., Yakir, D., Zaehle, S., Reichstein, M., 2021. The three major axes of
682 terrestrial ecosystem function. Nature 598, 468–472. https://doi.org/10.1038/s41586-021-
683 03939-9
684 Musavi, T., Migliavacca, M., Reichstein, M., Kattge, J., Wirth, C., Black, T.A., Janssens, I.,
685 Knohl, A., Loustau, D., Roupsard, O., Varlagin, A., Rambal, S., Cescatti, A., Gianelle,
686 D., Kondo, H., Tamrakar, R., Mahecha, M.D., 2017. Stand age and species richness
687 dampen interannual variation of ecosystem-level photosynthetic capacity. Nat. Ecol.
688 Evol. 1, 1–7. https://doi.org/10.1038/s41559-016-0048
689 Norby, R.J., Warren, J.M., Iversen, C.M., Medlyn, B.E., McMurtrie, R.E., 2010. CO2
690 enhancement of forest productivity constrained by limited nitrogen availability. Proc.
691 Natl. Acad. Sci. 107, 19368–19373. https://doi.org/10.1073/pnas.1006463107
692 Novick, K.A., Biederman, J.A., Desai, A.R., Litvak, M.E., Moore, D.J.P., Scott, R.L., Torn,
693 M.S., 2018. The AmeriFlux network: A coalition of the willing. Agric. For. Meteorol.
694 249, 444–456. https://doi.org/10.1016/j.agrformet.2017.10.009
695 Novick, K.A., Ficklin, D.L., Stoy, P.C., Williams, C.A., Bohrer, G., Oishi, A.C., Papuga, S.A.,
696 Blanken, P.D., Noormets, A., Sulman, B.N., Scott, R.L., Wang, L., Phillips, R.P., 2016.
697 The increasing importance of atmospheric demand for ecosystem water and carbon
698 fluxes. Nat. Clim. Change 6, 1023–1027. https://doi.org/10.1038/nclimate3114
699 Odum, E.P., 1969. The Strategy of Ecosystem Development. Science 164, 262–270.
700 https://doi.org/10.1126/science.164.3877.262
701 Pan, Y., Birdsey, R.A., Fang, J., Houghton, R., Kauppi, P.E., Kurz, W.A., Phillips, O.L.,
702 Shvidenko, A., Lewis, S.L., Canadell, J.G., Ciais, P., Jackson, R.B., Pacala, S.W.,
703 McGuire, A.D., Piao, S., Rautiainen, A., Sitch, S., Hayes, D., 2011. A Large and
704 Persistent Carbon Sink in the World's Forests. Science 333, 988–993.
705 https://doi.org/10.1126/science.1201609

706 Park Williams, A., Allen, C.D., Macalady, A.K., Griffin, D., Woodhouse, C.A., Meko, D.M.,
707 Swetnam, T.W., Rauscher, S.A., Seager, R., Grissino-Mayer, H.D., Dean, J.S., Cook,
708 E.R., Gangodagamage, C., Cai, M., McDowell, N.G., 2013. Temperature as a potent
709 driver of regional forest drought stress and tree mortality. Nat. Clim. Change 3, 292–297.
710 https://doi.org/10.1038/nclimate1693
711 Pugh, T.A.M., Lindeskog, M., Smith, B., Poulter, B., Arneth, A., Haverd, V., Calle, L., 2019.
712 Role of forest regrowth in global carbon sink dynamics. Proc. Natl. Acad. Sci. 116,
713 4382–4387. https://doi.org/10.1073/pnas.1810512116
714 Rebmann, C., Aubinet, M., Schmid, H., Arriga, N., Aurela, M., Burba, G., Clement, R., De
715 Ligne, A., Fratini, G., Gielen, B., Grace, J., Graf, A., Gross, P., Haapanala, S., Herbst,
716 M., Hörtnagl, L., Ibrom, A., Joly, L., Kljun, N., Kolle, O., Kowalski, A., Lindroth, A.,
717 Loustau, D., Mammarella, I., Mauder, M., Merbold, L., Metzger, S., Mölder, M.,
718 Montagnani, L., Papale, D., Pavelka, M., Peichl, M., Roland, M., Serrano-Ortiz, P.,
719 Siebicke, L., Steinbrecher, R., Tuovinen, J.-P., Vesala, T., Wohlfahrt, G., Franz, D.,
720 2018. ICOS eddy covariance flux-station site setup: a review. Int. Agrophysics 32, 471–
721 494. https://doi.org/10.1515/intag-2017-0044
722 Reich, P.B., Hobbie, S.E., Lee, T.D., Pastore, M.A., 2018. Unexpected reversal of C3 versus C4
723 grass response to elevated CO2 during a 20-year field experiment. Science 360, 317–320.
724 https://doi.org/10.1126/science.aas9313
725 Rogers, A., Medlyn, B.E., Dukes, J.S., 2014. Improving representation of photosynthesis in
726 Earth System Models. New Phytol. 204, 12–14. https://doi.org/10.1111/nph.12972
727 Saxe, H., Ellsworth, D.S., Heath, J., 1998. Tree and forest functioning in an enriched CO2
728 atmosphere. New Phytol. 139, 395–436. https://doi.org/10.1046/j.1469-
729 8137.1998.00221.x
730 Sitch, S., Friedlingstein, P., Gruber, N., Jones, S.D., Murray-Tortarolo, G., Ahlström, A., Doney,
731 S.C., Graven, H., Heinze, C., Huntingford, C., Levis, S., Levy, P.E., Lomas, M., Poulter,
732 B., Viovy, N., Zaehle, S., Zeng, N., Arneth, A., Bonan, G., Bopp, L., Canadell, J.G.,
733 Chevallier, F., Ciais, P., Ellis, R., Gloor, M., Peylin, P., Piao, S.L., Le Quéré, C., Smith,
734 B., Zhu, Z., Myneni, R., 2015. Recent trends and drivers of regional sources and sinks of
735 carbon dioxide. Biogeosciences 12, 653–679. https://doi.org/10.5194/bg-12-653-2015

736 Sutton, M.A., Simpson, D., Levy, P.E., Smith, R.I., Reis, S., Van OIJEN, M., De VRIES, W.,
737 2008. Uncertainties in the relationship between atmospheric nitrogen deposition and
738 forest carbon sequestration. Glob. Change Biol. 14, 2057–2063.
739 https://doi.org/10.1111/j.1365-2486.2008.01636.x
740 Thum, T., Caldararu, S., Engel, J., Kern, M., Pallandt, M., Schnur, R., Yu, L., Zaehle, S., 2019.
741 A new model of the coupled carbon, nitrogen, and phosphorus cycles in the terrestrial
742 biosphere (QUINCY v1.0; revision 1996). Geosci. Model Dev. 12, 4781–4802.
743 https://doi.org/10.5194/gmd-12-4781-2019
744 Tramontana, G., Jung, M., Schwalm, C.R., Ichii, K., Camps-Valls, G., Ráduly, B., Reichstein,
745 M., Arain, M.A., Cescatti, A., Kiely, G., Merbold, L., Serrano-Ortiz, P., Sickert, S., Wolf,
746 S., Papale, D., 2016. Predicting carbon dioxide and energy fluxes across global
747 FLUXNET sites with regression algorithms. Biogeosciences 13, 4291–4313.
748 https://doi.org/10.5194/bg-13-4291-2016
749 Ueyama, M., Ichii, K., Kobayashi, H., Kumagai, T., Beringer, J., Merbold, L., Euskirchen, E.S.,
750 Hirano, T., Marchesini, L.B., Baldocchi, D., Saitoh, T.M., Mizoguchi, Y., Ono, K., Kim,
751 J., Varlagin, A., Kang, M., Shimizu, T., Kosugi, Y., Bret-Harte, M.S., Machimura, T.,
752 Matsuura, Y., Ohta, T., Takagi, K., Takanashi, S., Yasuda, Y., 2020. Inferring CO2
753 fertilization effect based on global monitoring land-atmosphere exchange with a
754 theoretical model. Environ. Res. Lett. 15, 084009. https://doi.org/10.1088/1748-
755 9326/ab79e5
756 Walker, A.P., Kauwe, M.G.D., Bastos, A., Belmecheri, S., Georgiou, K., Keeling, R.F.,
757 McMahon, S.M., Medlyn, B.E., Moore, D.J.P., Norby, R.J., Zaehle, S., Anderson-
758 Teixeira, K.J., Battipaglia, G., Brienen, R.J.W., Cabugao, K.G., Cailleret, M., Campbell,
759 E., Canadell, J.G., Ciais, P., Craig, M.E., Ellsworth, D.S., Farquhar, G.D., Fatichi, S.,
760 Fisher, J.B., Frank, D.C., Graven, H., Gu, L., Haverd, V., Heilman, K., Heimann, M.,
761 Hungate, B.A., Iversen, C.M., Joos, F., Jiang, M., Keenan, T.F., Knauer, J., Körner, C.,
762 Leshyk, V.O., Leuzinger, S., Liu, Y., MacBean, N., Malhi, Y., McVicar, T.R., Penuelas,
763 J., Pongratz, J., Powell, A.S., Riutta, T., Sabot, M.E.B., Schleucher, J., Sitch, S., Smith,
764 W.K., Sulman, B., Taylor, B., Terrer, C., Torn, M.S., Treseder, K.K., Trugman, A.T.,
765 Trumbore, S.E., Mantgem, P.J. van, Voelker, S.L., Whelan, M.E., Zuidema, P.A., 2021.

766 Integrating the evidence for a terrestrial carbon sink caused by increasing atmospheric
767 CO2. New Phytol. 229, 2413–2445. https://doi.org/10.1111/nph.16866
768 Yu, X., Orth, R., Reichstein, M., Bahn, M., Klosterhalfen, A., Knohl, A., Koebsch, F.,
769 Migliavacca, M., Mund, M., Nelson, J.A., Stocker, B.D., Walther, S., Bastos, A., 2022.
770 Contrasting drought legacy effects on gross primary productivity in a mixed versus pure
771 beech forest. Biogeosciences 19, 4315–4329. https://doi.org/10.5194/bg-19-4315-2022
772 Zaehle, S., Sitch, S., Smith, B., Hatterman, F., 2005. Effects of parameter uncertainties on the
773 modeling of terrestrial biosphere dynamics. Glob. Biogeochem. Cycles 19.
774 https://doi.org/10.1029/2004GB002395
775 Zhan, C., Orth, R., Migliavacca, M., Zaehle, S., Reichstein, M., Engel, J., Rammig, A., Winkler,
776 A.J., 2022. Emergence of the physiological effects of elevated CO2 on land–atmosphere
777 exchange of carbon and water. Glob. Change Biol. 28, 7313–7326.
778 https://doi.org/10.1111/gcb.16397
779